

## Structure of nanoparticles in the $ZrO_2$ – $Y_2O_3$ system, as obtained under hydrothermal conditions

A. I. Shuklina<sup>1</sup>, A. V. Smirnov<sup>2</sup>, B. A. Fedorov<sup>2</sup>, S. A. Kirillova<sup>1</sup>, O. V. Almjashaeva<sup>3</sup>

<sup>1</sup>Saint Petersburg State Electrotechnical University “LETI”,  
ul. Professora Popova, 5, Saint Petersburg, 197376, Russia

<sup>2</sup>ITMO University, Kronverksky Pr. 49, bldg. A, Saint Petersburg, 197101, Russia

<sup>3</sup>Ioffe Institute, Politekhnikeskaya St. 26, Saint Petersburg, 194021, Russia  
almjasheva@mail.ru

PACS 61.46.+w, 81.40.-z

DOI 10.17586/2220-8054-2020-11-6-729-738

It is shown that monocrystalline nanoparticles with fluorite structure are formed in the  $ZrO_2$ – $Y_2O_3$  system, under hydrothermal conditions. The limiting content of  $Y_2O_3$  in the nanocrystals based on zirconium dioxide is 21.7–22.6 mol.%. Yttrium oxide not included in the structure forms an amorphous phase, which is stable even upon thermal treatment at 1000–1300 °C. It has been found that under hydrothermal conditions the structure of the nanocrystals based on  $ZrO_2(Y_2O_3)$  solid solution includes water, its content depending on yttrium oxide concentration in the solid solution.

**Keywords:** nanocrystals, hydrothermal synthesis, solid solution, zirconia.

*Received:* 10 August 2020

*Revised:* 15 October 2020

### 1. Introduction

Due to the presence of several polymorphic modifications [1–4] zirconium dioxide is of interest as a model for studying the effect of the synthesis methods and parameters on the formation of nanocrystals with different structure [5–15]. Zirconium dioxide based nanomaterials with various structures, morphologies, and particle size parameters have a wide range of applications [16–27], which makes the above studies relevant from a practical point of view as well.

In particular, papers [20, 21] show the perspective of using the photoelectrodes based on nanocrystals formed in the  $ZrO_2$ – $Y_2O_3$  system in perovskite solar cells. At the same time, it is noted in these works that the change in the band gap in such materials may depend not only on their composition, but also on the features of the nanoparticle structure [20, 21]. As known, the band gap and other properties of functional materials can be sensitive to the methods and parameters of synthesis [5–12, 23, 28–32]. As mentioned in papers [28–30], one of the specific features of formation of the nanoparticles based on solid solutions in the  $ZrO_2$ – $M_2O_3$  ( $M = Gd_2O_3, Y_2O_3, In_2O_3$ ) systems is the possibility of forming the nanoparticles with a “core-shell” structure. Studying the possibility of forming the nanoparticles with a particular structure and particular dimensional parameters, depending on the method and conditions of synthesis, will make it possible to intentionally synthesize the nanoparticles with the required properties.

The perspectives of using the  $ZrO_2(Y_2O_3)$  nanocrystals to convert solar energy necessitate a systematic study of the formation processes of nanomaterials with a certain structure, morphology and dimension parameters of the particles. The present study is aimed at solving these issues.

### 2. Experimental part

Zirconium dioxide based nanoparticles in the  $ZrO_2$ – $Y_2O_3$  system were obtained, in a wide range of the components’ ratios, by dehydration of co-precipitated hydroxides under hydrothermal conditions, according to the method described in [6].

The precipitation was carried out from a mixture of aqueous solutions of zirconium oxychloride ( $ZrOCl_2 \cdot 8H_2O$ , chemically pure (TU 6-09-3677-74)) and yttrium chloride ( $YCl_3 \cdot 6H_2O$ , pure (TU 6-09-4773-79)), with 12 M ammonium hydroxide solution ( $NH_4OH$ , reagent grade (GOST 3760-79)). The obtained precipitates were rinsed with distilled water and dried at a temperature of 100 °C. Hydrothermal treatment was carried out at a temperature  $T = 250$  °C and pressure  $P = 70$  MPa. Time of the hydrothermal treatment was recorded according to the duration of isothermal holding of autoclaves in the furnace. The duration of isothermal holding was 4 h.

The elemental composition was determined by energy-dispersive X-ray spectroscopy (EDS) with the use of a scanning electron microscope (Hitachi S-570) with energy-dispersive analyzer (Bruker Quantax 220).

The structural state of the samples and the parameters of the unit cells were determined from the data of X-ray powder diffraction obtained using Shimadzu XRD-7000 X-ray diffractometer. Diffractograms were taken using  $\text{CuK}\alpha$  radiation in the range of angles  $2\theta$  from 10 to 60 °C. When determining the unit cell parameters of compounds in the samples, silicon was introduced as an internal standard.

To study the structural changes during heating, the Shimadzu XRD-7000 diffractometer is equipped with a high temperature furnace (Anton Paar HTN 1200 K). The sample was air-heated from room temperature to 1100 °C, with a stop after every 100 °C. At each temperature step, the isothermal holding time was 10 min.

Dimensional parameters of the crystallites were determined from the data on the X-ray diffraction lines' profile. The crystallites' distribution was determined using software (SmartLabStudio II). Average dimensions of the crystallites were calculated using the Scherrer formula and also data on the crystallites' size distribution.

The dimensional characteristics of nanoparticles were determined from the data of small-angle X-ray scattering [33, 34]. Two methods were applied for the calculation, i.e. the "Guinier method" [33] and the method of "standard curves" [34]. The small-angle measurements were made using Kratky block-camera.  $\text{CuK}\alpha$  radiation was used. The absorption factor of the sample was determined using an attachment with a moving slit.

The pycnometric density was measured by helium pycnometry, using the gas pycnometer Ultra Pycnometer 1000 (Quanta Chrome). For measurements, all the samples were pre-dried at 100 °C for 30 minutes. The measurements were carried out in a 10 cm<sup>3</sup> cell, with preliminary degassing of the sample for 5 min. in stream mode. The number of consecutive measurements was 10, the preset limit of measurement error was maximum 0.01 g/cm<sup>3</sup>.

Thermal transformations were studied by differential scanning calorimetry combined with thermogravimetric analysis, using the thermal analyzer NETZSCH (STA 429CD).

### 3. Results and discussion

The results of elemental analysis showed that, subject to the method sensitivity limits, there were no elements other than Zr, Y, O. According to EDS analysis, subject to error limits of the method, the ratio of elements, in terms of the oxides  $\text{ZrO}_2$  and  $\text{Y}_2\text{O}_3$ , corresponded to (nominal) composition of the samples specified for the synthesis, as shown in Table 1.

TABLE 1. Results of elemental analysis of the samples based on the system  $\text{ZrO}_2\text{-Y}_2\text{O}_3$

Content of $\text{YO}_{1.5}$ in the system, mol.%	
Nominal composition	EDS
5	5.0
8	8.6
12	12.0
15	16.4
20	19.7
25	23.3
30	31.0
45	46.4
55	57.2

According to X-ray diffraction analysis, all the samples obtained by co-precipitation of the components were X-ray amorphous. After their hydrothermal treatment at 250 °C, for 4 h, at  $\text{Y}_2\text{O}_3$  content in the samples of up to 46.4 mol.%, zirconium dioxide based phases with fluorite structure (Fig. 1a) were formed. For the sample containing 57.2 mol.%  $\text{Y}_2\text{O}_3$ , narrow peaks corresponding to  $\text{Y}(\text{OH})_3$  were recorded (Fig. 1b) against the background of X-ray maxima corresponding to the zirconium dioxide based phase with fluorite structure.

Based on the X-ray diffraction data, parameter values of the unit cell of the zirconium dioxide based phase with fluorite structure were calculated, and the unit cell parameter was plotted against the amount of yttrium oxide in the system (Fig. 2). The obtained values correlate well with literature data, up to the  $\text{Y}_2\text{O}_3$  content in the system corresponding to 19.7 mol.%, and can be described by a linear relationship:

$$a(x) = a_0 + \alpha \cdot x, \quad (1)$$

where  $a$  is a parameter of the cubic unit cell of the phase based on zirconium dioxide with fluorite structure;  $x$  is content of  $\text{YO}_{1.5}$  in the system  $\text{ZrO}_2\text{-YO}_{1.5}$ , expressed in mole fractions;  $a_0 = 5.116 \pm 0.004 \text{ \AA}$ ,  $\alpha = 0.29 \text{ \AA/mole}$

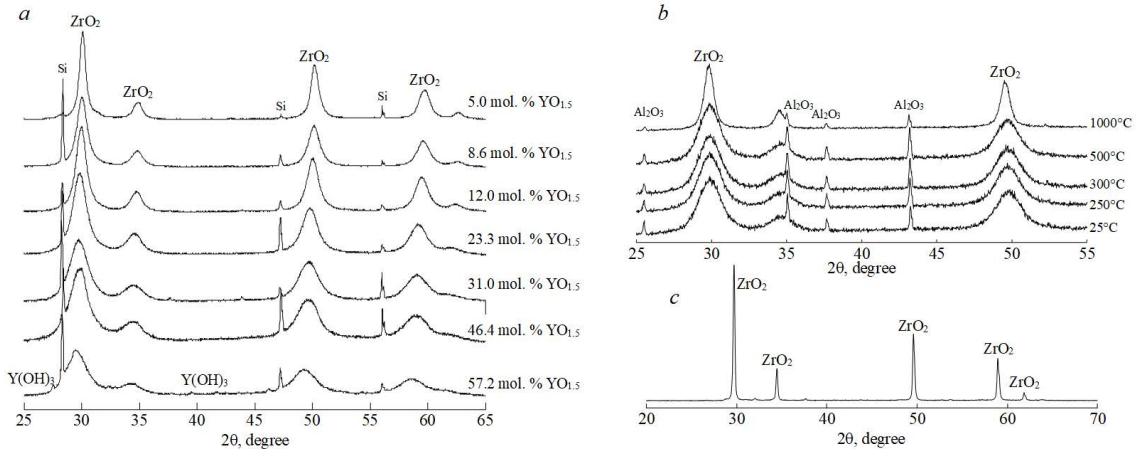


FIG. 1. X-ray diffractograms of the samples in the system  $ZrO_2$ - $YO_{1.5}$ : (a) samples obtained by hydrothermal treatment of co-precipitated hydroxides at  $T = 250\text{ }^\circ\text{C}$ ,  $P = 70\text{ MPa}$ ,  $\tau = 4\text{ h}$  (Si – peaks of the internal standard); (b) the sample containing 31.0 mol.%  $Y_2O_3$ , after heat treatment during high temperature X-ray diffraction ( $Al_2O_3$  – peaks of the high temperature cell); (c) the sample containing 46.4 mol.%  $Y_2O_3$ , after additional heat treatment by air at  $T = 1300\text{ }^\circ\text{C}$

fractions. However, starting from  $YO_{1.5}$  content in the system of 19.7 mol.%, the dependence of  $a(x)$  greatly deviates from the straight line (1), actually taking the following form in the range 31.0–46.4 mol.%  $Y_2O_3$ :

$$a(x) = a_\infty, \tag{2}$$

where  $a_\infty$  is a constant, which in this case equals to the value  $a_\infty = 5.178 \pm 0.002$ .

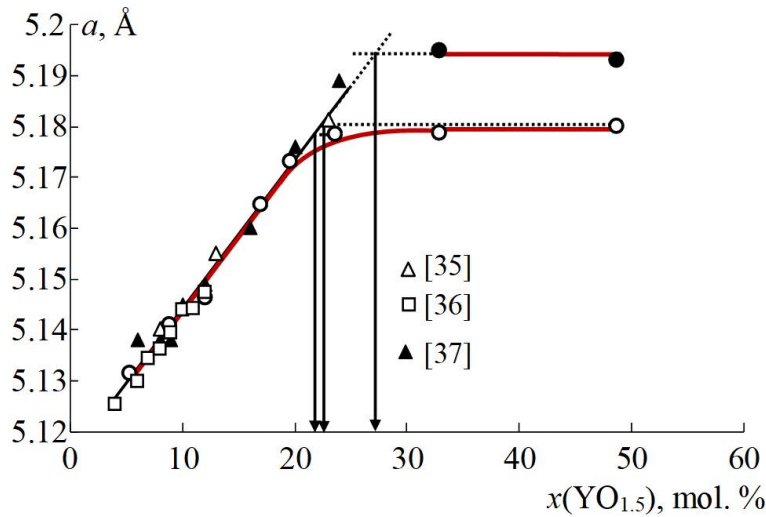
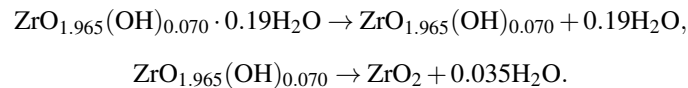


FIG. 2. Unit cell parameter vs. amount of yttrium oxide in the system

The independence of the unit cell parameter on the phase composition indicates that increasing of yttrium oxide content in the system does not lead to increase in its concentration in the phase of variable composition –  $Zr_{(1-x)}Y_xO_{(2-0.5x)}$ . The fact that in this range of compositions the X-ray diffractogram does not show any other crystalline phases leads one to conclude that yttrium oxide not included in the structure of the variable composition phase based on zirconium dioxide is in X-ray amorphous state. In papers [28, 29] this state was classified as a state of yttrium oxide in the X-ray amorphous shell surrounding nanocrystalline particles. Thus, in the range of  $Y_2O_3$  content of 23.3 to 46.4 mol.%, a noticeable amount of amorphous phase can be expected in the system, since the concentration  $Y_2O_3$  in these samples, as calculated from the data on the unit cell parameter values, varies in the range 21.7–22.6 mol.%, i.e. differs from the system composition.

After high temperature treatment, the X-ray diffraction data (Fig. 1) showed that the system comprising 31.0 and 46.4 mol.%  $Y_2O_3$  did not contain any other crystalline phases except for the phase of variable composition with fluorite structure. Meanwhile, based on the data on the unit cell parameter values of the variable composition phase  $Zr_{(1-x)}Y_xO_{(2-0.5x)}$  with fluorite structure for these samples (Fig. 2.), we can conclude that yttrium oxide concentration therein equals to  $x \approx 0.272$  mole fractions ( $\approx 27.2$  mol.%  $Y_2O_3$ ), i.e. significantly less than the content of yttrium oxide in the system. Thus, even after thermal treatment a significant portion of yttrium oxide remains in the X-ray amorphous state. However, based on the state diagram of the system  $ZrO_2$ – $Y_2O_3$  [1–4] we could expect yttrium oxide entering the solid solution at a treatment temperature of 1000–1300 °C. Apparently, insufficient thermal treatment time does not allow the formation of  $Zr_{(1-x)}Y_xO_{(2-0.5x)}$  phase with fluorite structure of equilibrium composition, and spatial constraints, presented as grains of the zirconium dioxide based phase with fluorite structure, do not allow the transformation of the amorphous phase based on yttrium oxide into crystalline one. The possibility of realizing such an effect was noted in [38] and was theoretically analyzed in [39].

As shown in [40], in the course of heat treatment nanocrystalline zirconium dioxide loses water in several stages, at different temperatures. However, the weight loss is associated not only with the removal of the surface adsorbed water, but also with composition change and with the corresponding structural transitions in the nanocrystals based on zirconium dioxide, in the temperature range 200–500 °C [40, 41]:



A similar situation, as Fig. 3 shows, is observed in the samples based on the system  $ZrO_2$ – $Y_2O_3$ . When studying the samples behavior by means of synchronous thermal analysis, prominent endothermic effect is observed in the range of temperatures of  $\sim 25$ – $150$  °C, which is accompanied by weight loss and corresponds to the removal of water adsorbed on the nanoparticles surface. At higher temperatures, two more steps of water loss in the samples are observed: in the range of temperatures of  $\sim 150$ – $570$  °C and  $\sim 570$ – $1120$  °C, respectively.

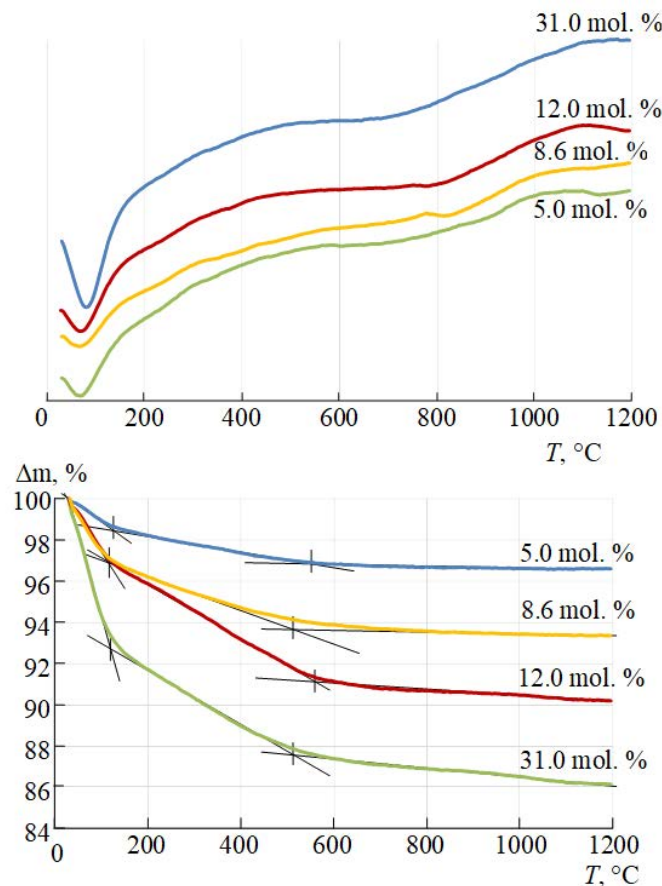


FIG. 3. Results of synchronous thermal analysis

Analysis of the thermogravimetric study results allowed us to conclude that the composition of the zirconium dioxide based nanoparticles obtained by hydrothermal treatment can be presented as a formula comprising a certain amount of chemically bound water:  $Zr_{(1-x)}Y_xO_{(2-0.5x)} \cdot nH_2O$ . The results of estimating the amount of chemically bound water, depending on the content of yttrium oxide in the system, are shown in Fig. 4. Considering the results of [41] relating to water state in the structure of nanoparticles based on zirconium dioxide, we can conclude that in the nanoparticles, where zirconium dioxide is partially substituted by yttrium oxide, water is presented both in the form of crystallization water with dehydration temperature range of  $\sim 150$ – $570$  °C, and in the form of constitution water – the temperature range of removal of  $\sim 570$ – $1120$  °C.

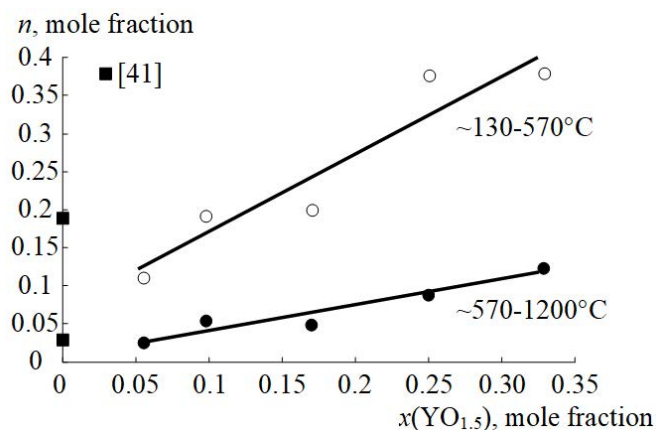


FIG. 4. Amount of water  $n_1(H_2O)$  and  $n_2(H_2O)$  ( $n_2(OH) = 2 \cdot n_2(H_2O)$ ) in the nanoparticles of variable composition ( $n_1(H_2O) + n_2(H_2O) = n(H_2O)$ ) vs. yttrium oxide content in the system

Considering the results of [41] relating to the hydrated state in the nanocrystals based on zirconium dioxide and the relationships shown in Fig. 4, or in the analytical form:

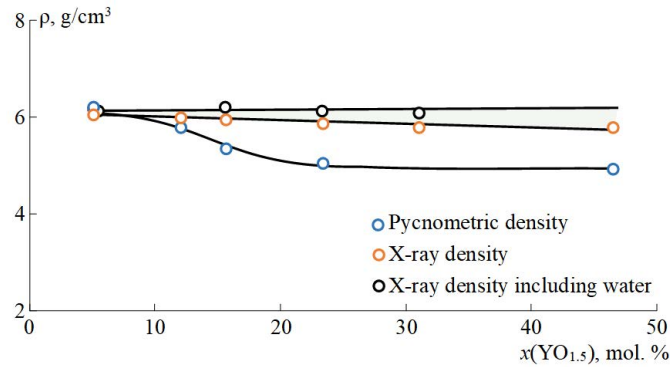
$$n_1(H_2O) = 0.07 + 1.022 \cdot x,$$

$$n_2(H_2O) = 0.012 + 0.325 \cdot x,$$

$$n_2(OH) = 2 \cdot n_2(H_2O) = 0.024 + 0.675 \cdot x,$$

where  $n_1$  is the amount of crystallization water, mole fractions;  $n_2$  is the amount of constitution water, mole fractions, ( $n(H_2O) = n_1(H_2O) + n_2(H_2O)$ ), the formula of the solid solution comprising yttrium oxide and water can be recorded as follows:  $Zr_{1-x}Y_xO_{2-0.5x-0.5(0.024+0.675 \cdot x)}OH_{(0.024+0.675 \cdot x)} \cdot (0.07 + 1.022 \cdot x)H_2O$ . The values obtained are in qualitative compliance with data presented in [41], wherein comprehensive studies by means of proton magnetic resonance, X-ray phase analysis and comprehensive thermal analysis were used to determine the composition of nanoparticles based on zirconium dioxide, expressed by the formula  $ZrO_{1.965}(OH)_{0.07} \cdot 0.19H_2O$ . Some quantitative differences between the chemical composition of a nanocrystalline zirconium dioxide based compound obtained for nanocrystals not containing yttrium oxide in the structure –  $ZrO_{1.965}(OH)_{0.07} \cdot 0.19H_2O$  [41], and the composition obtained by extrapolation  $x \rightarrow 0$  of the expression  $Zr_{1-x}Y_xO_{1.988-0.838x}OH_{(0.024+0.675 \cdot x)} \cdot (0.07 + 1.022 \cdot x)H_2O$ , i.e.  $ZrO_{1.988}OH_{0.024} \cdot 0.07H_2O$ , are apparently due to their structural differences. In the case described in [41], the nanocrystals have a structure close to tetragonal one, which is stabilized by water entry into the lattice. The paper discusses the case of nanocrystals of solid solutions based on zirconium dioxide, whose structure is described as a cubic one, stabilized by the substitution of zirconium ions by yttrium ions in the crystal lattice, with charge compensation in the anion sublattice.

The density of the samples was determined by the method of helium pycnometry, in comparison with the X-ray density shown in Fig. 5. The X-ray density of the crystalline samples was determined from data on the volume of the unit cells and their elemental composition, with and without regard for water included in their structure. Based on the analysis of the relationship in Fig. 5, it can be concluded that as the yttrium oxide amount in the system increases, the values of pycnometric density of the samples somewhat decrease as compared with the X-ray density, calculated both with and without regard for water in the structure. This is most likely due to the presence in the samples enriched with yttrium oxide, especially at a content of  $x > 19.7$  mol.%, where, under hydrothermal synthesis conditions, an amorphous phase is produced that is enriched with hydrated forms of yttrium oxide having significantly lower density than zirconium dioxide based crystalline phases of interest. Since the substance density decreases

FIG. 5. Samples density vs. amount of  $Y_2O_3$ 

during the transition to the amorphous state [42, 43], the density of hydrated forms of yttrium oxide can be estimated as:  $\rho(YOOH) < 4.48 - 4.63 \text{ g/cm}^3$  [44–46],  $\rho(Y(OH)_3) < 3.80 - 3.90 \text{ g/cm}^3$  [44, 47–49].

Based on the analysis of data obtained by small-angle X-ray scattering, size distribution of the particles was determined, and mean values of the particle sizes were calculated (Table 2). Data in Fig. 6 show that as yttrium oxide amount in the system increases, both mean dimensions of crystallites and mean dimensions of particles decrease remarkably. Almost complete matching, within error limits, of the mean dimensions of crystallites and particles (except for the point at 46.4 mol.% of  $Y_2O_3$ ) indicates that the obtained nanoparticles are predominantly monocrystalline. Comparison of the size distribution curves of crystallites and particles (Fig. 7) shows their similar nature. In both cases, there is a tendency towards narrowing of the sizes distribution region and shifting of the size distribution maxima towards smaller sizes both of particles and crystallites, as yttrium oxide content in the system increases, and this is another proof of the above conclusion about monocrystalline nature of the nanoparticles, which is irrespective of the size thereof.

TABLE 2. Results of the study by means of small-angle X-ray analysis

$Y_2O_3$ content in the sample	Particle diameter, nm		Particle surface per unit volume, $m^2/cm^3$  $(S/V)_{particle}$	Density*)	Specific surface
	standard curve method $D$	Guinier method $D_r$		$\rho$	$S_{specific}$
5.0	$12.0 \pm 0.2$	$11.98 \pm 0.05$	$917 \pm 39$	6.21	$151 \pm 9$
8.6	$8.90 \pm 0.04$	$8.77 \pm 0.06$	$1224 \pm 3$	6.19	$197 \pm 5$
16.4	$8.26 \pm 0.06$	$8.29 \pm 0.04$	$1400 \pm 2$	6.17	$225 \pm 3$
23.3	$7.92 \pm 0.8$	$7.84 \pm 0.06$	$1539 \pm 8$	6.14	$248 \pm 2$
31.0	$5.9 \pm 0.2$	$5.7 \pm 0.1$	$1777 \pm 47$	6.12	$293 \pm 7$
46.4	$9.7 \pm 0.6$	$9.4 \pm 0.1$	$1571 \pm 12$	6.11	$254 \pm 5$
57.2	$5.12 \pm 0.06$	$5.08 \pm 0.04$	$1887 \pm 32$	6.06	$309 \pm 3$

\*) X-ray density with regard for water included in the structure

Based on the data on the particle size and their X-ray density with regard for water included in the structure, specific surface areas of the samples were calculated (Fig. 8).

Note the inverse relationship between the samples' specific surface areas on the one hand and the size of nanoparticles and the content of yttrium oxide in the system on the other. This is due to the fact that the nanoparticle sizes themselves steadily decrease as the amount of yttrium oxide in the samples increases. The nature of the relationship between water adsorbed on the nanoparticles' surface on the one hand and their specific surface areas and  $Y_2O_3$  content in the system on the other (Fig. 9) is explained similarly.

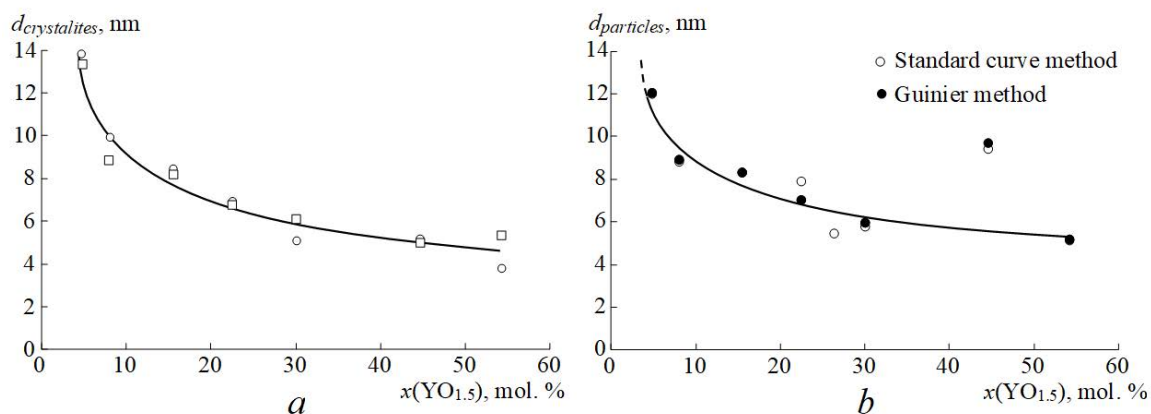


FIG. 6. Crystallite (a) and particles (b) size in the system  $ZrO_2$ - $Y_2O_3$  vs. amount of yttrium oxide

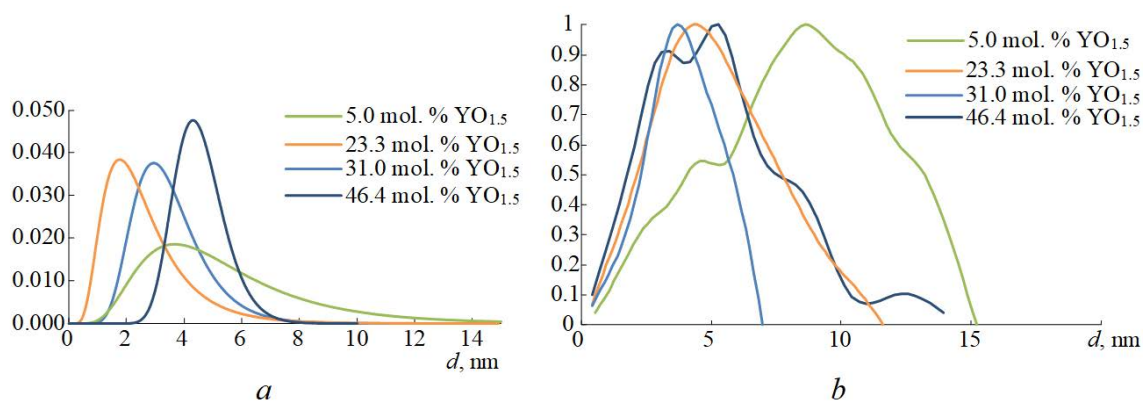


FIG. 7. Size distribution of crystallites (a) and particles (b)

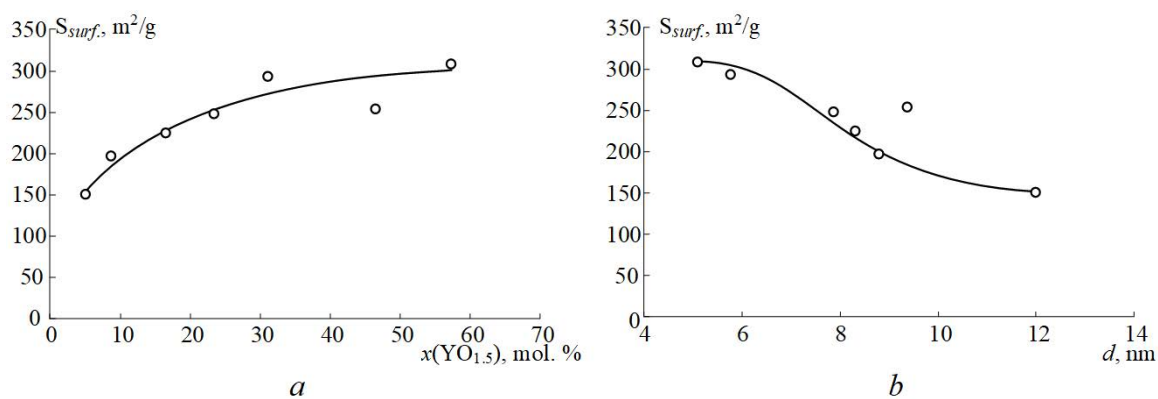


FIG. 8. Specific surface areas of the samples vs composition (a) and size (b) of the particles

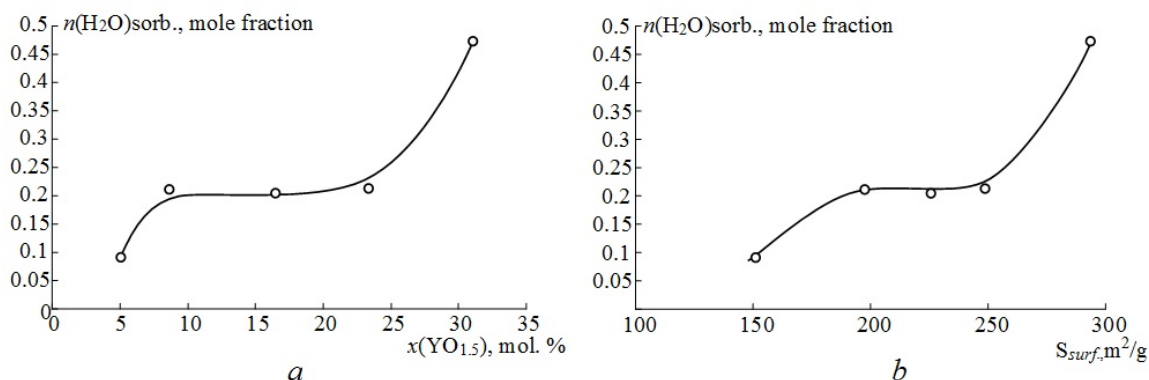


FIG. 9. Amount of water adsorbed on the surface of nanoparticles vs. their specific surface areas and amount of yttrium oxide in the system

#### 4. Conclusion

The study showed that nanocrystalline particles are formed in the  $\text{ZrO}_2\text{--Y}_2\text{O}_3$  system under hydrothermal conditions, with the particle size decreasing as yttrium oxide content in the system increases. The limiting content of  $\text{Y}_2\text{O}_3$  in the nanocrystals based on zirconium dioxide with fluorite-like structure is 21.7–22.6 mol.%, when they are formed by hydrothermal treatment of co-precipitated hydroxides at  $T = 250\text{ }^\circ\text{C}$ , pressure  $P = 70\text{ MPa}$ , for 4 h. Yttrium oxide not included in the structure forms an amorphous phase, stable even upon high-temperature treatment of the samples. It is shown that under hydrothermal conditions the structure of nanocrystals based on  $\text{ZrO}_2(\text{Y}_2\text{O}_3)$  solid solution includes water, its content depending on yttrium oxide concentration in the solid solution. Comparison of the data on the crystallites' and particles' size distribution showed that the nanoparticles formed under hydrothermal conditions are monocrystalline structures.

#### Acknowledgments

The authors express their gratitude to V. V. Gusarov for the attention he paid to the work.

X-ray diffraction and SEM/EDS was performed using the equipment of the Engineering Center Saint Petersburg State Institute of Technology.

This study was financially supported by the Russian Science Foundation (project no. 20-63-47016).

#### References

- [1] Degtyarev S.A., Voronin G.F. Solution of ill-posed problems in thermodynamics of phase equilibria. The  $\text{ZrO}_2\text{--Y}_2\text{O}_3$  system. *Calphad*, 1988, **12**(1), P. 73–82.
- [2] Stubican V.S., Hink R.C., Ray S.P. Phase equilibria and ordering in the system  $\text{ZrO}_2\text{--Y}_2\text{O}_3$ . *J. Am. Ceram. Soc.*, 1978, **61**(1-2), P. 17–21.
- [3] Srivastava K.K., Patil R.N., Choudhary C.B., Gokhale K.V.G.K., Subbarao E.C. Revised phase diagram of the system  $\text{ZrO}_2\text{--YO}_{1.5}$ . *Trans. J. Br. Ceram. Soc.*, 1974, **73**(5), P. 85–91.
- [4] Andrievskaya E.R. Phase equilibria in the refractory oxide systems of zirconia, hafnia and yttria with rare-earth oxides. *J. Eur. Ceram. Soc.*, 2008, **28**, P. 2363–2388.
- [5] Bugrov A.N., Almjasheva O.V. Effect of hydrothermal synthesis conditions on the morphology of  $\text{ZrO}_2$  nanoparticles. *Nanosystems: Physics, Chemistry, Mathematics*, 2013, **4**(6), P. 810.
- [6] Pozhidaeva O.V., Korytkova E.N., Drozdova I.A., Gusarov V.V. Phase state and particle size of ultradispersed zirconium dioxide as influenced by condition of hydrothermal synthesis. *Russian Journal of General Chemistry*, 1999, **69**(8), P. 1219–1222.
- [7] Yapyrintsev A.D., Baranchikov A.E., Gubanova N.N., Ivanov V.K., Tret'yakov Yu.D. Synthesis of nanocrystalline  $\text{ZrO}_2$  with tailored phase composition and microstructure under high-power sonication. *Inorganic Materials*, 2012, **48**(5), P. 494–499.
- [8] Wang H., Li G., Xue Y., Li L. Hydrated surface structure and its impacts on the stabilization of t- $\text{ZrO}_2$ . *Journal of Solid State Chemistry*, 2007, **180**(10), P. 2790–2797.
- [9] Meskin P.E., Gavrilov A.I., Maksimov V.D., Ivanov V.K., Churagulov B.R. Hydrothermal/microwave and hydrothermal/ultrasonic synthesis of nanocrystalline titania, zirconia, and hafnia. *Russian Journal of Inorganic Chemistry*, 2007, **52**(11), P. 1648–1656.
- [10] Ivanov V.K., Baranov A.N., Oleinikov N.N., Tret'yakov Y.D. Fractal Surfaces of  $\text{ZrO}_2$ ,  $\text{WO}_3$  and  $\text{CeO}_2$ . Powders. *Inorganic materials*, 2002, **38**(12), P. 1224–1227.
- [11] Taguchi M., Nakaneb T., Matsushita A., Sakkab Y., Uchikoshib T., Funazukuria T., Nakab T. One-pot synthesis of monoclinic  $\text{ZrO}_2$  nanocrystals under subcritical hydrothermal conditions. *The Journal of Supercritical Fluids*, 2014, **85**, P. 57–61.
- [12] Stenina I.A., Voropaeva E.Y., Veresov A.G., Kapustin G.I., Yaroslavtsev A.B. Effect of precipitation pH and heat treatment on the properties of hydrous zirconium dioxide. *Russian Journal of Inorganic Chemistry*, 2008, **53**(3), P. 350–356.
- [13] Glushkova, V.B., Lapshin, A.V., Vershinin, A.A. et al. Phase formation of zirconia-based solid solutions synthesized from peroxides. *Glass Physics and Chemistry*, 2004, **30**(6), P. 558–563.

- [14] Zhang Y., Li A., Yan Z., Xu G., Liao C., Yan C.  $(ZrO_2)_{0.85}(ReO_{1.5})_{0.15}$  (Re = Sc, Y) solid solutions prepared via three Pechini-type gel routes: 1-gel formation and calcination behaviors. *Journal of Solid State Chemistry*, 2003, **171**, P. 434–438.
- [15] Popov V.V., Menushenkov A.P., Yastrebtev A.A., Arzhatkina L.A., Tsarenko N.A., Shchetinin I.V., Zheleznyi M.V., Ponkratov K.V. Regularities of formation of complex oxides with the fluorite structure in the  $ZrO_2$ - $Y_2O_3$  system. *Russian Journal of Inorganic Chemistry*, 2017, **62**(9), P. 1147–1154.
- [16] Almjasheva O.V., Gusarov V.V., Danilevich Ya.B., Kovalenko A.N., Ugolkov V.L. Nanocrystals of  $ZrO_2$  as sorption heat accumulators. *Glass Physics and Chemistry*, 2007, **33**(6), P. 587–589.
- [17] Fokin B.S., Belenkiy M.Ya., Almjashev V.I., Khabensky V.B., Almjasheva O.V., Gusarov V.V. Critical heat flux in a boiling aqueous dispersion of nanoparticles. *Technical Physics Letters*, 2009, **35**(5), P. 440–442.
- [18] Kablov E.N., Stolyarova V.L., Vorozhtcov V.A., Lopatin S.I., Karachevtsev F.N. Thermodynamics and vaporization of ceramics based on the  $Y_2O_3$ - $ZrO_2$  system studied by KEMS. *Journal of Alloys and Compounds*, 2019, **794**, P. 606–614.
- [19] Bugrov A.N., Smyslov R.Yu., Zavialova A.Yu., Kopitsa G.P. The influence of chemical prehistory on the structure, photoluminescent properties, surface and biological characteristics of  $Zr_{0.98}Eu_{0.02}O_{1.99}$  nanophosphors. *Nanosystems: Physics, Chemistry, Mathematics*, 2019, **10**(2), P. 164–175.
- [20] Vildanova M.F., Nikolskaia A.B., Kozlov S.S., Karyagina O.K., Larina L.L., Shevaleevskiy O.I., Almjasheva O.V., Gusarov V.V. Nanostructured  $ZrO_2$ - $Y_2O_3$ -based system for perovskite solar cells. *Doklady Physical Chemistry*, 2019, **484**(2), P. 36–38.
- [21] Larina L.L., Alexeeva O.V., Almjasheva O.V., V.V. Gusarov, Kozlov S.S., Nikolskaia A.B., Vildanova M.F., Shevaleevskiy O.I. Very wide-bandgap nanostructured metal oxide materials for perovskite solar cells. *Nanosystems: Physics, Chemistry, Mathematics*, 2019, **10**(1), P. 70–74.
- [22] Zadorozhnaya O.Y., Napochatov Y.K., Agarkova E.A., Tiunova O.V. Layered solid-electrolyte membranes based on zirconia: production technology. *Russian Journal of Electrochemistry*, 2020, **56**(2), P. 124–131.
- [23] Kalitina, E.G., Pikalova, E.Y. Preparation and properties of stable suspensions of  $ZrO_2$ - $Y_2O_3$  powders with different particle sizes for electrophoretic deposition. *Inorganic Materials*, 2020, **56**(9), P. 941–948.
- [24] Rylski A., Siczek K. The effect of addition of nanoparticles, especially  $ZrO_2$ -based, on tribological behavior of lubricants. *Lubricants*, 2020, **8**(3), P. 1–25.
- [25] Hu C., Sun J., Long C., Wu L., Zhou C., Zhang X. Synthesis of nano zirconium oxide and its application in dentistry. *Nanotechnol Rev.*, 2019, **8**(1), P. 396–404.
- [26] Bumajdad A., Nazeer A.A., Al Sagheer F, Nahar S. Zaki Mohamed I. Controlled synthesis of  $ZrO_2$  nanoparticles with tailored size, morphology and crystal phases via organic/inorganic hybrid films. *Scientific Reports*, 2018, **8**, P. 3695.
- [27] Precious-Ayanwale A, Donohué-Cornejo A., Cuevas-González J.C., Espinosa-Cristóbal L.F., Reyes-López S.Y. Review of the synthesis, characterization and application of zirconia mixed metal oxide nanoparticles. *International Journal of Research – GRANTHAALAYAH*, 2018, **6**(8), P. 136–145.
- [28] Almjasheva O.V., Smirnov A.V., Fedorov B. A., Tomkovich M.V., Gusarov V.V. Structural features of  $ZrO_2$ - $Y_2O_3$  and  $ZrO_2$ - $Gd_2O_3$  nanoparticles formed under hydrothermal conditions. *Russian Journal of General Chemistry*, 2014, **84**(5), P. 804–809.
- [29] Almjasheva O.V., Krasilin A.A., Gusarov V.V. Formation mechanism of core-shell nanocrystals obtained via dehydration of coprecipitated hydroxides at hydrothermal conditions. *Nanosystems: Physics, Chemistry, Mathematics*, 2018, **9**(4), P. 568–572.
- [30] Tomkovich M.V., Andrievskaya E.R., Gusarov V.V. Formation under hydrothermal condition and structural features of nanoparticles based on the system  $ZrO_2$  -  $Gd_2O_3$ . *Nanosystems: Physics, Chemistry, Mathematics*, 2011, **2**(2), P. 139.
- [31] Enikeeva M.O., Kenges K.M., Proskurina O.V., Danilovich D.P., Gusarov V.V. Influence of hydrothermal treatment conditions on the formation of lanthanum orthophosphate nanoparticles of monazite structure. *Russian Journal of Applied Chemistry*, 2020, **93**(4), P. 540–548.
- [32] Popkov V.I., Bachina A.K., Valeeva A.A., Lobinsky A.A., Gerasimov E.Y., Rempel A.A. Synthesis, morphology and electrochemical properties of spherulite titania nanocrystals. *Ceramics International*, 46(15), P. 24483–24487.
- [33] Guinier A., Fournet G. *Small-angle Scattering of X-rays*. New-York, Wiley, 1955. 268 .
- [34] Kuchko A.V., Smirnov A.V. The computation of the nanoparticles volume distribution function and the specific surface area based on the small-angle x-ray scattering indicatrix by the meyhod of the statistical regularization. *Nanosystems: Physics, Chemistry, Mathematics*, 2012, **3**(3), P. 76–91.
- [35] Fabregas I.O., Craievich A.F., Fantini M.C.A., Millen R.P., Temperini M.L.A, Lamas D.G. Tetragonal-cubic phase boundary in nanocrystalline  $ZrO_2$ - $Y_2O_3$  solid solutions synthesized by gel-combustion. *Journal of Alloys and Compounds*, 2011, **509**, P. 5177–5182.
- [36] Dell'Agli G., Mascolo G. Hydrothermal synthesis of  $ZrO_2$ - $Y_2O_3$  solid solutions at low temperature. *J. Eur. Ceram. Soc.*, 2000, **20**(2), P. 139–145.
- [37] Kim D.-J. Lattice parameters, ionic conductivities, and solubility limits in fluorite-structure  $MO_2$  oxide [M =  $Hf^{4+}$ ,  $Zr^{4+}$ ,  $Ce^{4+}$ ,  $Th^{4+}$ ,  $U^{4+}$ ] solid solutions. *J. Am. Ceram. Soc.*, 1989, **72**(8), P. 1415–1421.
- [38] Almjasheva O.V., Gusarov V.V. Hydrothermal synthesis of nanosized and amorphous alumina in the  $ZrO_2$ - $Al_2O_3$ - $H_2O$  system. *Russian Journal Inorganic Chemistry*, 2007, **52**(8), P. 1194–1200.
- [39] Al'myashev O.V., Gusarov V.V. Features of the phase formation in the nanocomposites. *Russian Journal of General Chemistry*, 2010, **80**(3), P. 385–390.
- [40] Al'myasheva O.V., Ugolkov V.L., Gusarov V.V. Thermochemical analysis of desorption and adsorption of water on the surface of zirconium dioxide nanoparticles. *Russian Journal of Applied Chemistry*, 2008, **81**(4), P. 609–613.
- [41] Almjasheva O.V., Denisova T.A. Water state in nanocrystals of zirconium dioxide prepared under hydrothermal conditions and its influence on structural transformations. *Russian Journal of General Chemistry*, 2017, **87**(1), P. 1–7.
- [42] Amorphous Metallic Alloys, Ed. by F.E. Lyuborsky (Butterworths, London, 1983; Metallurgiya, Moscow, 1987).
- [43] Gabelkov S.V., Tarasov R.V., Poltavtsev N.S., Logvinkov D.S., Mironova A.G. Phase transformation in the nanocrystallization of amorphous zirconium oxide. *Questions of atomic science and technology. Series: Physics of radiation damage and radiation materials science 2004*, **3**, P. 116–120. (in Russian)
- [44] Klevtsov P.V., Klevtsova R.F., Sheina L.P. Crystalline yttrium hydroxides. *Journal of Structural Chemistry*, 1965, **5**(4), P. 536–541.
- [45] Klevtsova R.F., Klevtsov P.V. The crystal structure of YOOH. *J. Struct. Chem.*, 1965, **5**, P. 795–797.
- [46] Christensen A.N. A Reinvestigation of the Crystal structure of YOOH. *Acta Chem. Scand*, 1965, **19**(6), P. 1504–1505.

- [47] Landolt-Börnstein – Group III Condensed Matter 7b1. Ed by K.-H. Hellwege, A.M. Hellwege – Key Element O. Part 1.1975, Springer-Verlag Berlin Heidelberg.
- [48] Christensen A.N., Hazell R.G., Nilsson A. Hydrothermal investigation of the systems  $Y_2O_3-H_2O-Na_2O$ ,  $Y_2O_3-D_2O-Na_2O$ ,  $Y_2O_3-H_2O$ , and  $Y_2O_3-H_2O-NH_3$ . *Acta Chem. Scand.*, 1967, **21**(2), P. 481–492.
- [49] Schubert K., Seitz A. Kristallstruktur von  $Y(OH)_3$ . *Zeitschrift für anorganische und allgemeine Chemie (ZAAC)*, 1947, **254**(12), P. 116–125.